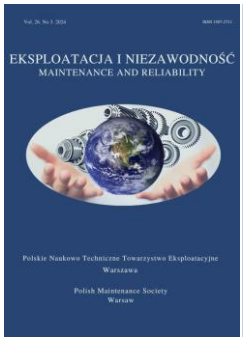

Eksploatacja i Niezawodnosc – Maintenance and Reliability
Volume 26 (2024), Issue 3
journal homepage: http://www.ein.org.pl

Article citation info:
Khan N, Khan R, Wieczorowski M, A. Alnaser I, H Seikh A, Haji Ya H, Reliability Assessment of Gored Elbow in Erosive Two-Phase Flow with Sand Particles, Eksploatacja i Niezawodnosc – Maintenance and Reliability 2024: 26(3) http://doi.org/10.17531/ein/190362

Reliability Assessment of Gored Elbow in Erosive Two-Phase Flow with Sand Particles

Indexed by:

Nauman Khan[a], Rehan Khan[a,*], Michał Wieczorowski[b], Ibrahim A. Alnaser[c], Asiful H Seikh[c], Hamdan Haji Ya[d]

[a] Department of Mechanical Engineering, College of Electrical and Mechanical Engineering,, National University of Sciences and Technology, Islamabad, Pakistan
[b] Faculty of Mechanical Engineering, Institute of Applied Mechanics, Poznan University of Technology, Poland
[c] Center of Excellence for Research in Engineering Materials (CEREM), Deanship of Scientific Research, College of Engineering, King Saud University, Riyadh 11421, Saudi Arabia
[d] Mechanical Engineering Department, Universiti Teknologi PETRONAS, Malaysia

Highlights

- The gored elbow can reduce erosion by 32% compared to the standard elbow.
- Gored elbows have low-velocity regions compared to the standard 90-degree elbow.
- The extent of erosion was assessed for gored 90 degrees.
- In erosive gas-solid flow, reliability can be enhanced by using a gored elbow.

Abstract

Erosion, a major threat to the safety and reliability of piping components, can significantly impact their integrity and functionality. This study employs computational fluid dynamics (CFD) to systematically investigate the erosion behavior of four elbow designs (standard 90-degree elbow, 18-degree gored elbow, 22.5-degree gored elbow, and 30-degree gored elbow) subjected to multiphase air-sand and water-sand flows. Our primary objective is to identify the optimal elbow design that effectively mitigates erosion and enhances the safety and reliability of piping systems. Our findings reveal that the 22.5-degree gored elbow exhibits significantly lower erosion rates compared to other designs, particularly in air-sand flows, making it the superior choice for reducing erosion by up to 32% compared to the standard elbow. However, the standard 90-degree elbow demonstrates greater erosion resistance in water-sand flows. This research contributes valuable insights for selecting the optimal elbow design in multiphase flow, ultimately enhancing the design and longevity of piping systems.

Keywords
erosion, multiphase flow, computational fluid dynamics (CFD), standard 90-degree elbow, gored elbow

1. Introduction

Elbow pipes or simply elbows are curved fittings that connect two pipes at an angle to change the direction of the fluid flow. They are commonly used in piping systems for a variety of industrial applications, such as oil and gas, petrochemical, and process manufacturing industries. Elbow pipes allow fluids to change direction around obstacles and in narrow spaces while increasing turbulence, pressure drop, and energy losses [1]. The pressure drop and energy losses in the elbows are influenced by the fluid velocity, pipe roughness, pipe diameter, bend radius, and bend angle. These parameters determine how the pressure and energy change in the elbow system with different intensities. Elbow pipes are versatile and can accommodate a wide range of

(*) Corresponding author.
E-mail addresses: N. Khan, dnaumankhan890@gmail.com, R. Khan (ORCID: 0009-0003-3597-6396) mrehan.khan@ceme.nust.edu.pk, M. Wieczorowski (ORCID: 0000-0001-7526-8368) michal.wieczorowski@put.poznan.pl, I. A. Alnaser (ORCID: 0000-0001-6325-8410) ianaser@ksu.edu.sa, A. H Seikh (ORCID: 0000-0003-4609-9256) aseikh@ksu.edu.sa, H. Haji Ya, hamdan.ya@utp.edu.my

fluids and boundary conditions due to their availability in various materials, sizes, and shapes [2, 3]. However, elbow pipes are prone to erosion due to high fluid velocities near the inner wall caused by the flow direction. Erosion occurs when a fluid carrying solid particles repeatedly impacts the surface of the material, causing wear [4]. Substantial wear and tear damage can lead to component failure, pipeline leakage, and other dangerous consequences. Research has demonstrated that components such as elbows, tees, valves, chokes, U-bends, and separators that cause rapid changes in flow direction are more susceptible to wear damage [5-8]. Elbows in pipeline systems experience erosion rates up to 50 times higher than straight pipes. The fluid changes direction at the elbow, which increases its speed, and this results in the particles striking the elbow wall with higher intensity, causing significant erosion [9].

The standard 90° bend is the most commonly used flow-changing device in the oil and gas industry [10]. Extensive research has been conducted to investigate the erosive wear behavior and mechanism of the standard 90° elbows using experimental and numerical methods [11]. In a study conducted by Khan et al. [12], a multi-layer paint modeling technique and computational fluid dynamics (CFD) were employed for erosion analysis distribution inside an elbow under liquid-solid flow conditions. It was observed that enhancing the slurry speed significantly changed the way particles impacted the wall, resulting in an increase in material loss in the underside of the elbow. Solnordal et al. [13] conducted a study to determine the wear rate of a standard 90° elbow under pneumatic conveying of sand particles using experimental and numerical approaches. They employed a surface profiler to measure the erosion depth of the elbow and then simulated the flow patterns and particle tracks using CFD and discrete phase model (DPM). Moreover, different particle-wall collision models were evaluated, and it was found that the rough wall model best fitted with the experimental data. Mazumder et al. [14] performed an experimental and computational analysis of elbow erosion in mixed-phase flow. Erosion rates of elbows were measured in an erosion test loop, and the fluid and particle flow were simulated using CFD. They concluded that the mechanistic model developed in their study could be used to estimate erosion in elbows in multiphase fluid flow, and could be used to optimize the elbow design.

Kesana et al. [15] conducted a comprehensive study to analyze the erosive wear tendencies induced by the mixed-phase interaction of air and sand particles traversing a standard elbow. Utilizing ultrasonic technology in conjunction with numerical simulations, the researcher quantified and replicated the dispersion and extent of erosive impact spanning the surface of the elbow. Additionally, the study explores the influence of particle size and hardness on erosion behavior. The research findings revealed the precise location and intensity of maximum erosion under diverse flow conditions and orientations. Erosion is a complex process that occurs due to the interaction between fluid flow and solid particles [16]. The primary mechanism of erosion is the impact of these particles on a material surface leading to material removal over time [17]. This impact generates mechanical forces that can cause material detachment, surface abrasion, and eventual degradation. The erosion wear mechanism depends on various factors such as the properties of the particles, the angle of incident, the fluid, the surface as well as the flow conditions [18, 19]. The research investigation found that the rate of erosion in a 90-degree horizontal elbow increases with carrier fluid velocity. The study also revealed that the erosion rate at different locations of the elbow bend is different, varying from 2.6 to 8.9 mm/year at the fluid speed of 2.5m/s, 4.0 to 11.2 mm/year at a fluid velocity of 3.5 m/s and 5.8 to 14.6 mm/year at a fluid velocity of 4 m/s [20].

Another influential parameter in the field of pipeline engineering is the design of elbows and pipelines, which play a crucial role in determining their erosion rates. One such study was performed by Duarte et al. [21] examining a vertex chamber in comparison to a standard 90° elbow. The basic geometric parameters such as pipe diameter, domain size, and curvature radius were kept constant. A semi-sphere was constructed at the opposite side of the inlet. This research work concluded that the erosion rate in the vertex chamber was considerably dropped and in the worst-case scenario it was half of that in the 90° elbow. In addition to that, the vortex chamber could have a longer life span due to the more even distribution of erodent particles' impact on its surface. A study dedicated to erosion mitigation was conducted, wherein Zhu et al. [22] investigated the effects of trapezoidal rib on the extrados of a 90° elbow to minimize erosion. The researcher validated their CFD erosion prediction with experimental data for a standard elbow. It was observed

that an elliptical erosion zone with a vee-shaped scar on the extrados of the elbow was caused by particle impacts; however, the rib itself also suffers erosion. The rib positioned at θ=25° achieved the highest reduction of elbow erosion peak by 31.4%. The position and velocity of the rib influence its erosion rate and protection effect. They also found that elbow erosion increased with higher particle mass loading. Considering the erosion rate and protection effect, the optimal choice was to install the rib at θ=25°.

Zhou et al. [23] conducted a study to examine how swirling flow can effectively mitigate elbow erosion in solid particle pipelines. The results show that the introduction of a twisted tape generates a swirling flow that more evenly disperses the solid particles within the pipeline, reducing the erosion rate of the elbow. Additionally, the effectiveness of this erosion reduction is greater when the twist ratio is lower and the twisted tape is positioned close to the elbow. As the gas velocity increases in the presence of swirling flow, particle impact energy rises and the collision mode transitions from sliding to direct. While the erosion rate of an elbow fitted with a twisted tape also increases with the gas velocity, the presence of swirling flow reduces the velocity exponent of the erosion rate to some degree. This study suggests a new approach to mitigating elbow erosion through swirling flow and provides insight into the erosion mechanism and factors.

Duarte et al. [24] conducted another investigation to evaluate the erosion resistance of different configurations within a dilute gas-solid multiphase flow context. These configurations comprised the plugged tee, vortex chamber, and a conventional 90° elbow. The study concludes that, with respect to erosion reduction, the plugged tee geometry surpasses both the vortex chamber and conventional elbow. However, it is recognized that the inherent flow dynamics of the plugged tee design exhibit limitations when addressing erosive processes under conditions of higher mass loading. As a solution in scenarios characterized by substantial mass loading, the vortex chamber elbow emerges as the optimal choice [24].

A novel study introduces an innovative pipe wall design aimed at reducing the erosion of 90° elbow [25]. The design involves twisting the pipe wall along the flow streamline direction, creating a swirling flow upstream of the elbow. This redistributes transported particles, preventing their concentration at a single point on the elbow, and leads to an erosion reduction of 33% on the 90-degree elbow using this novel pipe wall configuration.

The literature on erosion mitigation strategies emphasizes the effectiveness of design modification in reducing elbow erosion. Although there is extensive research on erosion mitigation strategies for piping systems, the knowledge about gored elbow erosion is still limited. As indicated by the literature, design modifications are effective in mitigating erosion in conventional elbows, but their application to gored elbows is a new and relatively unexplored area.

Gored or segmented elbows have the unique characteristic of being made up of segments that can be customized in terms of size and shape, providing opportunities for innovative erosion mitigation methods. However, the current body of literature on erosion in gored elbows is limited, resulting in a lack of understanding of erosion patterns, underlying mechanisms, and optimal mitigation techniques for these specific components. The various dimensions and configurations of gored elbows, including parameters such as bend angle, segment angle, segment length, and segment diameter, have a significant impact on erosion behavior. Additionally, the different combinations of quantities and arrangements, such as three-segment, four-segment, and five-segment gored elbows, introduced complex factors that require further investigation.

The main objective of the current study is to investigate the anti-erosive behavior and reliability of gored elbows in comparison to the standard 90° elbow in multiphase flow conditions. To provide a focused investigation while maintaining a manageable scope, this study specifically examines 18-degree, 22.5-degree, and 30-degree gored elbows, representing a range of commonly used bend angles in various applications. The CFD-DPM simulation was adopted to predict the performance of elbow designs. The effects of carrier flow velocity, particle size, and the geometrical arrangement of the segment for liquid-solid and gas-solid flow are discussed.

This article follows a structured approach. In section 2, we detail the methodology, including geometry description, grid generation, numerical modeling, and validation. In section 3 we present and discuss the erosion behavior of the elbows under various flow conditions, including erosion rate analysis and

particle trajectories in air-sand and water-sand flows. Finally, in section 4 we conclude the article by summarizing the key findings and their implications.

2. Materials and Methods

2.1. Geometry description

The 3D model, as shown in Figure 1 was created using the SOLIDWORKS software. The geometric parameters for the simulations were selected based on the findings detailed in Vieira et al. [33]. The fluid flow enters through an initial straight section of 1000 mm in length, which includes a 90° elbow with a radius-to-diameter (r/D) ratio of 1.5. After the elbow, there is a subsequent straight segment of 600 mm in length to accommodate the outflow of the fluid. The inner diameter (D) of the pipe is fixed at 76.2 mm, as specified in Figure 1(a).

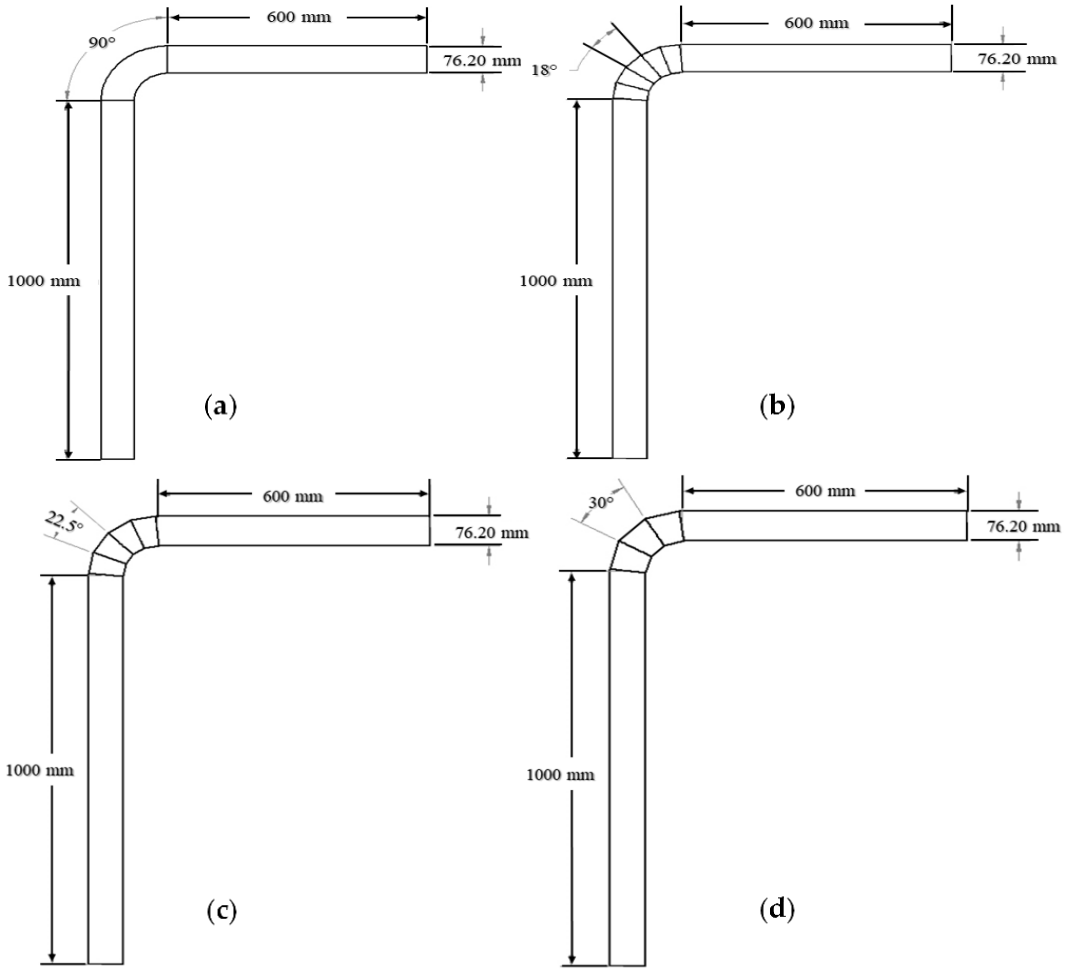

Fig. 1. (a) Geometry Dimensions of the Standard 90° Elbow (b), Gored Elbow with Five 18° Segments. (c) Gored elbow with four 22.5° segments (d), and Gored elbow with three 30° segments.

Figures 1(b), (c), and (d), illustrate three alternative geometries that have been modified from the main model. These geometries have different elbow curvatures, which are known as “gored” or “segmented” elbows in fluid dynamics. The first alternative geometry has an elbow with five segments, each with an 18° angle. The second alternative configuration has an elbow with four segments, each with a 22.5° angle. The third alternative structure has an elbow with three segments, each with a 30° angle. These geometries were used for comparative analysis of the simulation results.

2.2. Grid generation

Grid generation is a critical step in computational modeling and simulations. It allows the representation of the physical system’s geometry within a computational domain by creating a mesh of points or cells that cover the domain and serves as the basis for numerical simulations. A mesh refining study is a process of testing different meshes with varying levels of refinement and comparing the results with a reference solution or experimental data. The error rate of each mesh is calculated

by comparing the results of each mesh with the result of the reference solution. The error rate is defined as the relative difference between the two solutions in terms of the maximum erosion rate.

To evaluate the accuracy and validity of our numerical simulations, seven different meshes were applied with varying levels of refinement to the standard 90-degree elbow geometry. The maximum erosion rate obtained from each mesh was compared with the finer meshes as well as with the previous experimental results reported by Vieira et al. [33]. The number of nodes in each mesh reneged from 450,000 to 1,960,102 and the maximum wear rate at a specified location was calculated for each mesh. The fluid flow field was divided and a structured hexahedral mesh was generated for each case. The mesh size and the corresponding maximum wear rate for each case are illustrated in Table 1.

Table 1. Maximum Erosion Rate for Various Meshes with Different Node Numbers.

Mesh	Number of Nodes	Maximum Erosion
S0	4.50E+05	1.20E-05
S1	7.74E+05	2.90E-05
S2	1.20E+06	4.30E-05
S3	1.33E+06	4.60E-05
S4	1.50E+06	4.90E-05
S5	1.72E+06	5.00E-05
S6	1.96E+06	5.03E-05

The final mesh S6 was considered as the benchmark or reference solution for the other meshes. It found that S5 had the lowest error rate of 0.6%, which means that it had a high accuracy in simulating the erosion rate. S4 had a slightly higher error rate of 2.6%, which means that it still had an acceptable accuracy. S3 had a higher error rate of 8.5%, which means that it had less precision and reliability. S2 had a higher error rate of 14.5%, and S1 had a higher error rate of 42.3%, which means that they had poor accuracy and consistency. S0 had an extremely high error rate of 76%, which means that it had very low accuracy and validity.

It was also found that S6 had a high computational cost compared to S5, which took less time to run due to its coarser resolution. Therefore, S5 was selected as the optimal mesh for our ongoing numerical analyses, as it struck an excellent balance between accuracy and efficiency. Moreover, the previous experimental data from the study of Vieira et al. [26] fits well with the numerical results of S5, which further validated our choice of mesh and simulation approach.

To generate the meshes for the different elbow geometries, ANSYS Meshing was used to construct hexahedral structured elements. The mesh size and quality were controlled by adjusting the number of divisions and the smoothing parameters. The relationship between the maximum erosion rate and the number of nodes was visualized on a graph as shown in Figure 2. The x-axis represented the number of nodes, while the y-axis represented the erosion rate. The graph indicated that the maximum wear rate increased with the number of nodes increased, but the increase diminished as the mesh became finer.

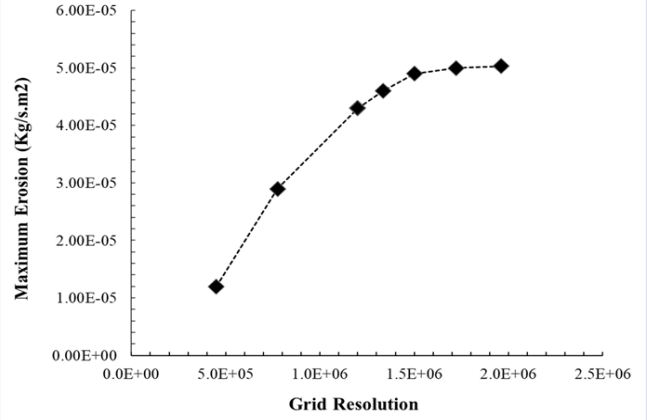

Fig. 2. Grid independent study: maximum erosion rate vs. node count.

Figure 3 displays the meshes of the elbow designs and their zoomed-in views, which demonstrates the uniformity and orthogonality of the elements in the region of interest.

The fluid flow problem was solved using the finite volume method. The pressure-velocity coupling was handled by the SIMPLE (Semi-Implicit Method for Pressure-Linked Equations) scheme, which is an iterative algorithm that alternates between guessing the pressure field and correcting the velocity field until convergence is achieved. The second-order upwind scheme was utilized for the discretization of the pressure, momentum, and turbulent kinetic energy equations. This scheme is more accurate and stable than the first-order upwind scheme, as it uses a higher-order polynomial interpolation.

The numerical method involved two different scenarios: one with air and the other with water as the continuous phases, both interacting with a discrete phase of sand particles. For the

continuous air phase, which had an air density of 1.225 kg/m³ and an air viscosity of 1.78× 10-5 kg/m-s, the boundary conditions were set as a velocity inlet and a pressure outlet. The simulation also adopted a standard wall function with no-slip conditions to model the interaction between the air and the pipe wall. The pipe wall material was stainless steel 316, with a density of 7990 kg/m³. Similarly, water was considered as the continuous phase in another scenario, with properties different from air. The density and viscosity of the water phase were set to 998.2 kg/m³, and 0.001003 kg/m-s respectively.

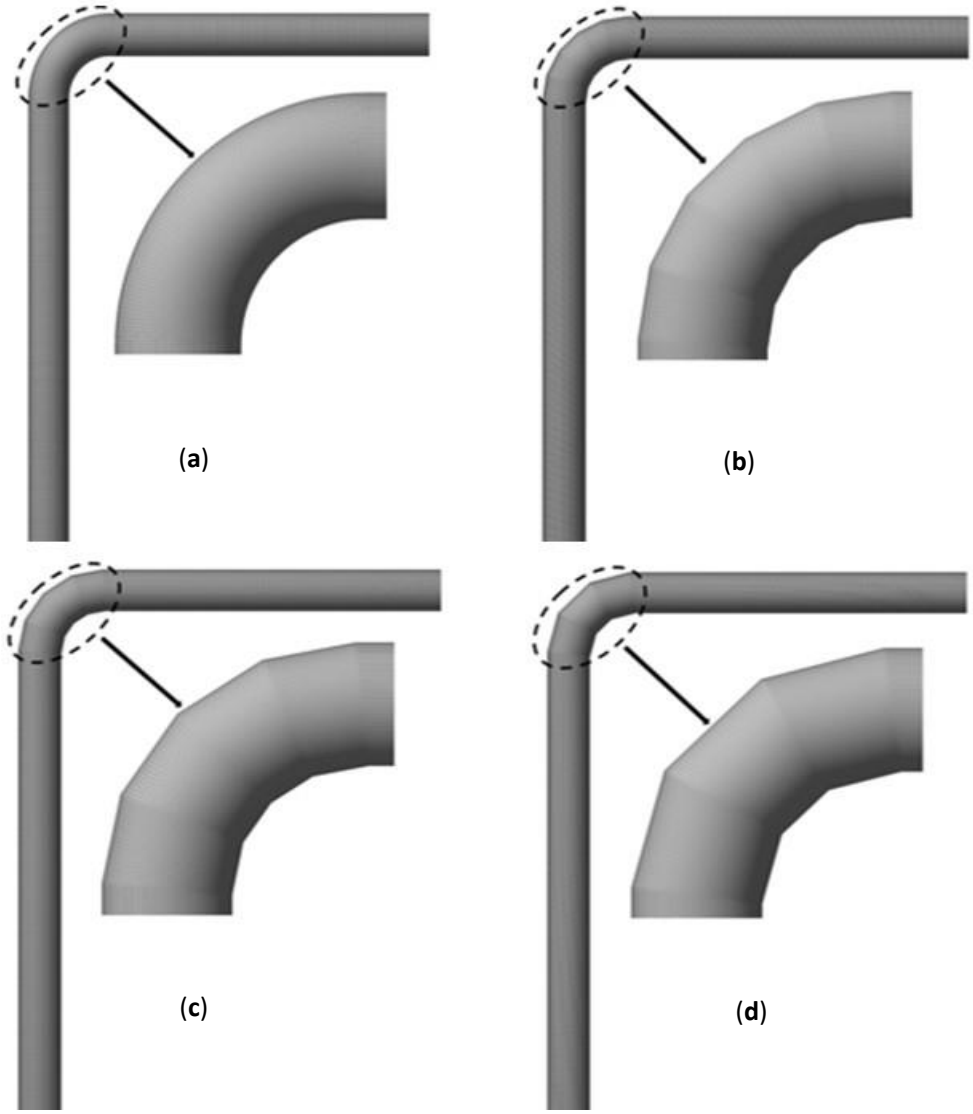

Fig. 3. (a) Mesh generated for the standard 90° elbow (b), Gored elbow with five 18° segments, (c) Gored elbow with four 22.5° segments (d), and gored elbow with three 30° segments.

In both cases, spherical sand particles composed primarily of angular SiO2-1 were introduced into the pipeline through the inlet. Different sand diameters were examined to understand the effect of particle size on transport and behavior within the respective continuous phases. The sand itself had a density of 2650 kg/m³, providing a wide range of properties for the analysis. Five CFD cases with different influencing parameters were set up for each design. The current analysis focuses on the specific operating conditions provided by Masters Pipes in Pakistan for their new hydrocarbon production plant pipeline. However, this paper recognizes the importance of developing generalizable design principles. Future research could explore how these findings might be adapted to a wider range of operating conditions, potentially through adjustments and additional considerations. This exploration would contribute to a more comprehensive understanding of pipeline design and benefit future projects beyond the specific case study. The influencing parameters included fluid speed, sand diameter, and sand flow rate as illustrated in Table 2.

Table 2. CFD cases and influencing parameters for air-sand and water-sand analysis.

Case	Velocity (m/s)	Particle Size (μm)	Sand Flow rate (kg/s)
1	10	200	0.05
2	12	225	0.065
3	15	250	0.08
4	18	275	0.095
5	20	300	0.1

For further analysis, two additional cases with higher values of the influencing parameters were created for each design to simulate the worst-case scenarios. The values for these two cases are shown in Table 3.

Table 3. Additional CFD cases with higher values of influencing parameters.

Case	Velocity (m/s)	Particle Size (μm)	Sand Flow rate (kg/s)
1	30	400	0.2
2	40	500	0.4

The present simulations provide valuable insight into elbow erosion resulting from sand particles. However, limitations arise due to the complex interaction of particle size, flow velocity, sand flow rate, and material properties. Accurately capturing these variables remains a formidable challenge. Future research could address this by expanding simulations or deriving generalized design principles. Currently, a detailed analysis specific to these simulations remains appropriate.

2.3. Numerical Modeling

Numerical modeling is a crucial tool for the in-depth study of the erosion phenomenon, which involves the complex processes of fluid flow, particle tracking, and erosion calculations. To simulate the interaction between air-sand and water-sand mixtures, the Eulerian-Lagrangian method is used. The Eulerian description focuses on the properties of the fluid at fixed points in space, while the Lagrangian description follows the trajectories of individual particles as they move through the fluid. The Euler-Lagrange approach solves the fluid equations on a fixed grid or mesh and tracks the particles using a discrete phase model (DPM). The advantage of this approach is that it can capture the complex interaction between fluid and particles, such as drag, lift, heat transfer, and collision. In the continuous phase model, governing equations for multiphase flow (air-sand or water-sand) are expressed through the Navier-Stokes equations for fluid motion. The flow characteristics of the continuous phase are determined by the continuity and momentum equations, which are represented as

$$\partial\rho/\partial t + \nabla(\rho\vec{u}\,) = 0 \quad (1)$$

$$\partial(\rho\vec{u}\,)/\partial t + \nabla(\rho\vec{u}\vec{u}\,) = -\nabla p + \nabla(\bar{\bar{\tau}}) + \rho g_i + S_D \quad (2)$$

In equations (1) and (2) ρ is the density of the fluid, and $\vec{u}$ is the velocity vector of the fluid, p is the static pressure, $\bar{\bar{\tau}}$ is the stress tensor, μ is the fluid viscosity, g_i is the gravitational acceleration, S_D is the additional source term due to interaction with the other phase. The equation of motion for a particle in a multiphase flow is expressed by the force balance:

$$m_p(d\vec{u}_p)/dt = \vec{F}_D + \vec{F}_G + \vec{F}_{VM} + \vec{F}_P \quad (3)$$

The equation in (3) includes the mass of the particles m_p, the drag force $\vec{F}_D$, the buoyancy force $\vec{F}_G$, the virtual mass force $\vec{F}_{VM}$, and the pressure gradient force $\vec{F}_P$. The k-epsilon (k-ε) model gives a general description of turbulence utilizing two transport equations: one for the turbulent kinetic energy (k), which represents the intensity of the turbulence; and one for the turbulent dissipation rate (ε), which represents the rate of energy loss due to viscosity. The equations are expressed as

$$(\partial(\rho k))/\partial t + \nabla\cdot(\rho k\boldsymbol{v}) = \nabla\cdot[(\mu + \mu_t/\sigma_k\,)\nabla k] - \rho k\omega + 2\mu_t S_{ij}S_{ij} - \rho/2\left(u_i u_j E_{ij}\right) \quad (4)$$

$$\partial(\rho\epsilon)/\partial t + \nabla\cdot(\rho\epsilon\boldsymbol{v}) = \nabla\cdot[(\mu + \mu_t/\sigma_\epsilon)\nabla\epsilon] - C_1\rho\epsilon\omega + C_2\rho\epsilon\omega^2 \quad (5)$$

In equation (4) k is the turbulent kinetic energy, *Sij* is the mean strain rate tensor, and *Eij* is the mean rotation rate tensor. In equation (5) ϵ denotes the turbulent dissipation rate and ω is the specific dissipation rate.

Numerous erosion models have been proposed by researchers to investigate and comprehend the impact of erosion in a numerical context. Notable models by Oka, Finnie, and McLaury serve as valuable blueprints for exploring erosion phenomena. The Oka erosion model [27] was chosen for both the air-sand and water-sand analysis in this research endeavor. This selection was motivated by the widespread adoption of this model within the research community and its notable alignment with empirical data. The Oka model is a semi-empirical model that accounts for particle impact velocity, impact angle, particle size, and material properties when predicting erosion rates. It offers a reasonable and effective method for quantitatively calculating erosion phenomena across a range of scenarios. It is a relatively simplified, but accurate model in many cases. The

Oka erosion model is represented by the following equation

$$E = E_0\left(v_p/v_{ref}\right)^{k_2}\left(D_p/D_{ref}\right)^{k_3} f(\theta) \quad (6)$$

In equation (3.6) E is the erosion rate, E_θ is the reference erosion rate at 90° impact angle, v_p is the particle impact velocity, v_{ref} is the reference impact velocity, D_p is the particle diameter, D_{ref} is the reference particle diameter, k_2 and k_3 are constant, and $f(\theta)$ is the impact angle function and given as

$$f(\theta) = (sin\,\alpha)^{n_1}\left(1 + H_v(1 - sin\,\alpha)\right)^{n_2} \quad (7)$$

For this investigation, the Oka erosion model utilized established reference values: 104 m/s for particle impact velocity, 326 µm for particle diameter, 1.049 Gpa for material hardness, and 2.3042 and 0.19 for constant k_2 and k_3, and constant n_1 and n_2 were assigned values of 0.7148 and 2.2945, respectively.

2.4. Validation of Results

This section presents the validation of the erosion rate in a conventional 90-degree elbow using numerical simulations. The Oka erosion model, which is suitable for this validation context, was used to perform the calculations for the numerical results. The experimental data obtained by Vieira et al. [33] were used as a benchmark to evaluate the accuracy of the numerical model. Four cases were selected from the experimental study, each considering different air speeds of 15 m/s and 23 m/s, sand sizes of 150 µm and 300 µm, and sand rates of 0.00274 kg/s, 0.00222 kg/s, 0.00297 kg/s, and 0.00263 kg/s as input parameters. The percentage error between the numerical and experimental results is also listed in Table 4.

Table 4. Numerical and Experimental evaluation of erosion rates in the 90-degree elbow.

Case	Air Speed (m/s)	Sand Size (µm)	Sand Rate (kg/s)	Experimental Thickness loss (mm/year)	CFD-simulated Thickness loss (mm/year)	% Error
1	15	150	0.00274	13.2	14.8	12.1
2	15	300	0.00222	19.3	21.9	13.5
3	23	150	0.00297	36.2	41.5	14.6
4	23	300	0.00263	80.3	94.7	17.9

Table 4 shows the cumulative thickness loss of the material due to erosion, expressed in millimeters per year (mm/year) or millimeters per day (mm/day), depending on the time scale of interest. We converted the erosion rate from kilograms per square meter per second (kg/m^2-s), which is the default unit in ANSYS fluent to millimeters per year, by dividing it by the density of the material (in kg/m^3). Thickness loss reflects the total material removed over a year or a day and serves as an indicator of erosion severity. The thickness loss in mm/year or mm/day can be calculated as follows;

$$Thickness\ Loss\ = Erosion\ Rate/density \quad (8)$$

The results show that the numerical model can capture the trends of erosion rate for the input parameters, and a good agreement was found between the numerical and experimental results. The percentage error was slightly higher for cases 3 and 4, where the air speed and sand rate were higher. A possible reason for this is the increased complexity of the erosion model in these conditions, which makes it harder to account for all the variables that affect erosion. Furthermore, the Oka erosion model predictions and experimental results differ because the model may not account for all the factors that affect erosion in these conditions and because the erosion predictions depend on the quality of the simulated flow field. More research is needed to improve the Oka erosion model for specific materials and flow or to use alternative models that are more accurate in these conditions. Moreover, the experimental data may have lower accuracy in these conditions, because of the challenges of measuring erosion rate at high velocities. However, it is noteworthy that the numerical results obtained by this study are significantly lower and closer to the experimental results of Vieira et al.[33] numerical results, indicating an improvement in the accuracy of the erosion rate predictions. The percentage error which remained below 20%, is still considered acceptable for this type of study. This confirms the validity and accuracy of the numerical model for predicting the erosion rate in a conventional 90-degree elbow.

The result reveals the relationship between specific parameters and erosion rates. It shows that erosion rates increase with increasing air velocity. This indicates the significant effect of air velocity on erosion phenomena under

the studied conditions. Likewise, sand size also influences erosion rates, with larger sand particles causing more erosion than smaller ones. This trend is illustrated in Table 4, which shows the erosion rates for two different sand sizes, specifically 150 and 300 micrometers, at an air velocity of 23 m/s. These results demonstrate the sensitivity of erosion rates to changes in air velocity and sand size, providing a useful reference for further analysis and design considerations in related applications.

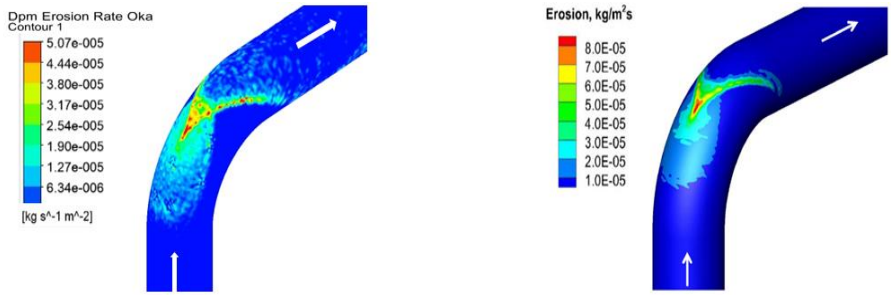

Fig. 4. Erosion rates for (a) 300 µm (Present Study), and (b) 300 µm (Vieira et al. [33]) sand sizes at 23 m/s air velocity.

The characteristic Elliptical and V-shaped erosion marks observed on the outer surface of the 90° elbow (Figure 4(a)) closely match those reported by Vieira et al. [33] (Figure 4(b)), strongly validating the accuracy of the present analysis. Moreover, the refined mesh throughout the domain likely contributes to the improved results presented in Figure 4(a) by enhancing the resolution of the physical system, capturing its complexities more accurately. This finer representation can lead to reduced numerical errors and improved capture of localized phenomena, eventually resulting in a distribution closer to estimated behavior and an average erosion rate that aligns better with experimental observations. Notably, as shown in Figure 4(a) compared to Figure 4(b), our model predicts a lower maximum erosion rate, potentially due to the refined mesh capturing the refinements of the erosion process and preventing the overestimation of localized erosion events.

3. Results and discussion

The numerical analysis of the erosion rate in air-sand flow in normal conditions and worst-case scenarios is presented in the subsequent section.

3.1. Erosion Rates Analysis of Air-Sand Flows.

Table 5 shows the results of the air-sand erosion simulations by ANSYS software on four elbow designs: a standard 90-degree elbow (Design 1), an 18-degree gored elbow (Design 2), a 22.5-degree gored elbow (Design 3), and a 30-degree gored elbow (Design 4). The simulations include varied velocity, particle size, and sand flow rate to evaluate erosion phenomena. The maximum erosion rates were estimated by the Oka model to compare erosion susceptibility across the designs.

Table 5. Maximum erosion rates for different elbow designs and factors in air-sand flow.

Case	Velocity (m/s)	Sand Size (µm)	Flow Rate (Kg/s)	Maximum Erosion Rate Oka (Kg/m2-s)			
				Design 1	Design 2	Design 3	Design 4
1	10	200	0.05	6.865E-05	9.070E-05	6.510E-05	7.269E-05
2	12	225	0.065	1.875E-04	1.787E-04	1.322E-04	1.632E-04
3	15	250	0.08	4.362E-04	4.358E-04	2.948E-04	4.244E-04
4	18	275	0.095	8.134E-04	7.533E-04	5.885E-04	7.805E-04
5	20	300	0.1	1.149E-03	1.151E-03	8.053E-04	1.029E-03

The result shows that for the first case, the 18-degree gored elbow (Design 2) has the highest erosion rate while the 22.5-degree gored elbow (Design 3) has the lowest erosion rate. This suggests that Design 2 is the most susceptible to erosion and Design 3 is the most resistant. Design 1 and 4 have comparable erosion rate values, with Design 4 slightly higher than Design 1. The results for case 2, as shown in Table 5 indicate that the 22.5-degree gored elbow (Design 3) has the lowest erosion rate in all designs. On the other hand, the standard 90-degree elbow (Design 1) has the highest erosion rate in all configurations. The erosion rate values of the 18-degree gored elbow (Design 2) and the 30-degree gored elbow (Design 4) are almost the same, but

Design 2 is a little higher than Design 4.

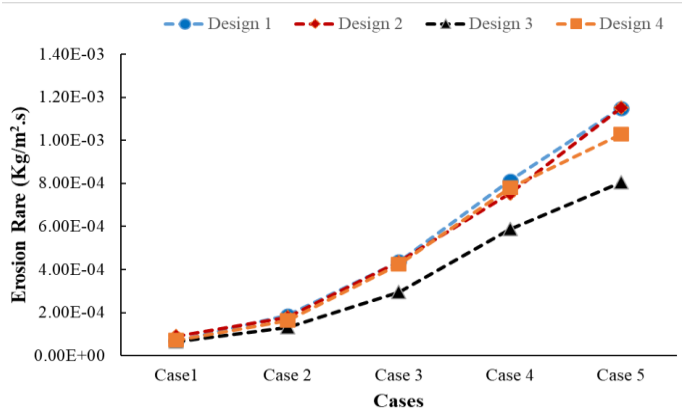

Fig. 5. Erosion rate trends for different elbow designs and air-sand operating conditions.

The results for cases 3 to 5, as presented in Table 5, confirm the outstanding erosion resistance of the 22.5-degree gored elbow (Design 3) in different conditions. This supports the idea that Design 3 is suitable for a wide range of operation conditions. The other designs have varying erosion rates, depending on bend angle and flow properties. Figure 5 illustrates the erosion rates for each case and design in a graphical way. The result displays the different erosion rate patterns for distinct elbow designs. Compared to the conventional 90-degree elbow (Design 1), represented by the blue curve, the 22.5-degree gored elbow (Design 3), indicated by the black curve, exhibits a higher erosion resistance. The other two designs, the 18-degree gored elbow (Design 2) and the 30-degree gored elbow (Design 4) have varying erosion rates compared to the conventional 90-degree elbow (Design 1). Depending on the conditions, they demonstrate slightly higher or lower erosion rates.

The average erosion rates for each pipeline design reveal significant insight into their performance under erosive conditions. Design 1, the standard 90-degree elbow, has an average erosion rate of 5.31E-04 Kg/m²-s, indicating its susceptibility to erosive wear. Design 2 shows a slightly reduced average erosion rate of 5.22E-04 Kg/m²-s, suggesting that some modifications in design can mitigate erosion. Design 3, presents the lowest average erosion rate of 3.77E-04 Kg/m²-s, highlighting its superior design in minimizing erosion. This could be attributed to the smoother flow transition and reduced particle impact energy due to the segment angles. Lastly, Design 4 has an average erosion rate of 4.94E-04 Kg/m²-s, which while better than Design 1, still indicates room for improvement compared to Design 3. These findings suggest that the Design 3 segmented approach significantly enhances the durability of the pipeline by reducing erosion rates, making it a potentially more reliable choice in air-sand applications.

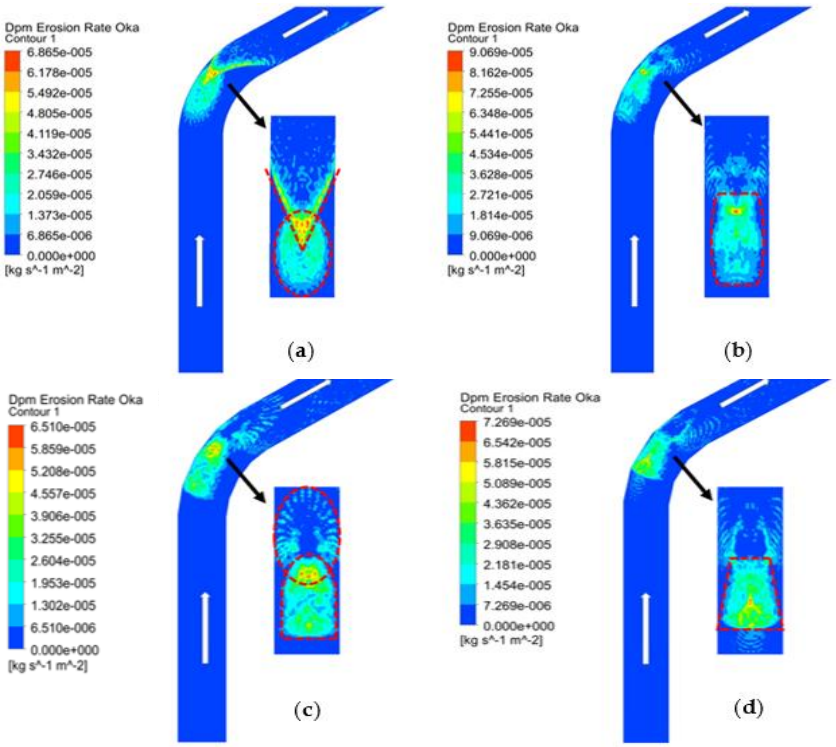

Fig. 6. Erosion rate of the (a) standard 90-degree elbow, (b) 18-degree gored elbow, (c) 22.5-degree gored elbow, (b) 30-degree gored elbow in air-sand flow for the first case (velocity=10 m/s, sand size=200μm, flow rate=0.05 kg/s).

A comparison of the erosion pattern of the 18-degree gored elbow, and the standard 90-degree elbow shows significant differences. The erosion scar in the 18-degree gored elbow is not elliptical; instead, it has a rectangular shape, with the larger sides slightly curved. Furthermore, in the case of the 18-degree gored elbow, as demonstrated in Figure 6 (b), a unique pattern of scattered and dispersed erosion points, which lack a clear shape, replaces the V-shaped scars of the standard 90-degree elbow. In contrast, the 22.5-degree gored elbow shows a cylindrical erosion scar with one straight side and one gently curved side, similar to a semicircular closed arch. Additionally, the upper surface of the elbow pipe exhibits an elliptical erosion scar, characterized by a hollow interior and formed by the dispersion of erosion points. These two distinct erosion patterns are illustrated in Figure 6(c). Finally, the 30-degree gored elbow demonstrates a trapezium-shaped erosion scar with a slightly rounded lower side and dispersed erosion points on the upper sections that do not form a specific shape, as shown in Figure 6 (d). The varying impact points of sand particles result in different erosion scar characteristics in each design. Moreover, the erosion scars indicate that areas more severe erosion occurs in areas with higher concentrations of sand particles. To determine the performance of each design under the worst-case scenario, the erosion rate was further examined by significantly increasing the influencing parameters. Table 6 lists the operating conditions and the maximum erosion rate for the two cases.

Table 6. Maximum erosion rates in worst-case scenarios for different elbow designs and factors in air-sand flow.

Case	Velocity (m/s)	Sand Size (μm)	Flow Rate (Kg/s)	Maximum Erosion Rate Oka (Kg/m2-s)			
				Design 1	Design 2	Design 3	Design 4
1	30	400	0.2	6.383E-03	7.041E-03	4.659E-03	5.971E-03
2	40	500	0.4	2.485E-02	2.906E-02	1.935E-02	2.615E-02

As Table 6 illustrates, the maximum erosion rate among various elbow designs. For case 1, Design 2, the 18-degree gored elbow, shows the highest maximum erosion, revealing its weakness to erosion compared to Design 1, the standard 90-degree elbow. In contrast, Design 3, the 22.5-degree gored elbow, has the least maximum erosion in all cases, showing its strength against erosion. Design 1 and Design 4, the 30-degree gored elbow have comparable erosion rates, with Design 1 slightly exceeding Design 4. For case 2, as Table 6 demonstrates, Design 3 keeps its low erosion rate among all designs. However, Design 2 has the most erosion in all cases. The erosion rates of Design 1 and Design 4 are nearly the same, with Design 4 slightly surpassing Design 1. Design 3, the 22.5-degree gored elbow, exhibits the lowest erosion rate in both cases, demonstrating, its erosion mitigation in the worst-case scenarios. Design 2, the 18-degree gored elbow, displays the highest erosion rate in both cases, indicating its susceptibility to erosion. The graphical comparison of the erosion rate across various cases and designs, illustrating the performance of each design, is presented in Figure 7. Figure 8 shows the erosion rates for the standard 90-degree elbow and 18-degree, the 22.5-degree and 30-degree gored elbows in the worst-case scenario for case 2.

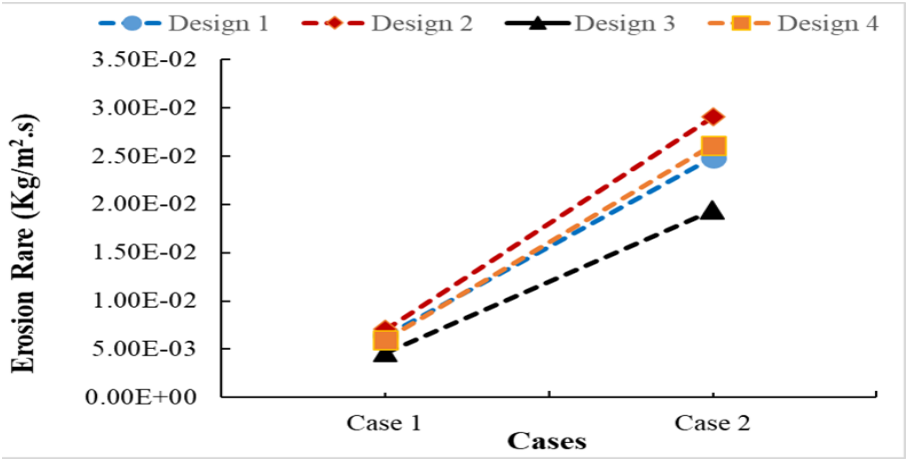

Fig. 7. Effect of elbow design on erosion rate in worst-case-scenario air-sand flow.

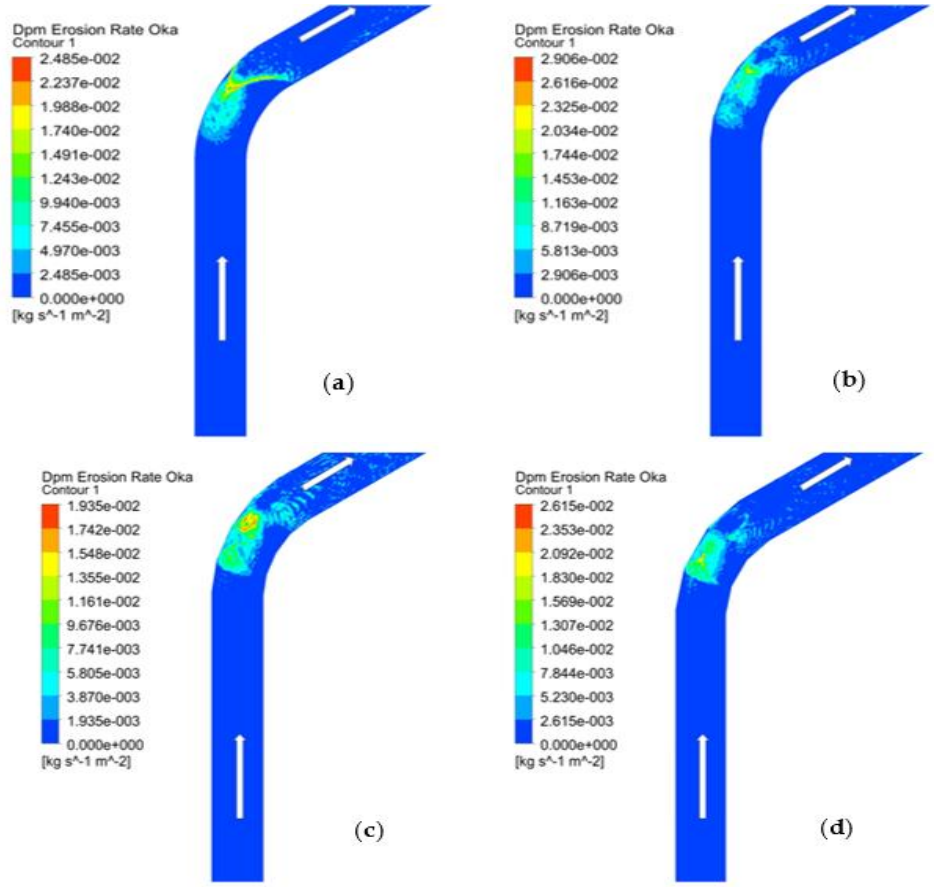

Fig. 8. Erosion rate of (a) standard 90-degree elbow, (b) 18-degree gored elbow (c) 22.5-degree gored elbow, (d) 30-degree gored elbow in a worst-case scenario, in air-sand flow (velocity=40 m/s, sand size=500μm, flow rate=0.4 kg/s).

Gored elbows, with their gentle curvature, offer a promising solution for mitigating erosion in air-sand flows compared to their sharp-angled 90-degree elbow. This improvement originates from several key factors. Firstly, the gored elbow design acts as a gradual transition, easing the flow direction change and reducing the harsh flow separation observed in 90-degree elbows. This transfer to smoother, more laminar flow with fewer eddies and vortices. Consequently, abrasive particle interactions with the elbow wall are minimized, leading to less wear. Additionally, the expanded flow area within the gored elbow reduces localized high-velocity zones near the inner surface, which is the main cause of severe erosion from sand particles.

Secondly, the curved surface of gored elbows alters the impact angle of sand particles. Compared to the head-on collision with a 90-degree elbow, particles meet a lower angle of the gored elbow segments. This has two beneficial effects: the normal component of particle velocity decreases, meaning the impact force acting perpendicular to the surface is less intense. Additionally, the glancing angle increases the likelihood of particle rebound, preventing them from lingering on the surface and causing increasing erosive damage. The result of this study suggests that the 22.5-degree gored elbow emerges as superior in terms of erosion reduction. This angle appears to achieve the optimal balance between flow streamlining and reduced particle impact, outperforming both the 18-degree and 30-degree elbow designs. The air-sand results show that the erosion rate in the gored elbows varies significantly depending on the case and the angle. The 18-degree gored elbow (Design 2) has the most erratic behavior, with erosion ranging from 0.95 to 1.32 times the standard 90-degree elbow. The 22.5-degree gored elbow (Design 30) exhibits the most consistent performance, with erosion decreasing in all cases, reaching up to 0.68 times the baseline. The 30-degree gored elbow (Design 4) has a moderate performance, with erosion mostly decreasing (0.87 to 0.97 times), except for one case where it slightly increases (1.06 times). The data demonstrate that the gored elbows have the potential to substantially reduce erosion (as in Design 3), but also the risk of unpredictable performance (as in Design 2) and,

in some cases even erosion enhancement (as in Design 4). Therefore, further investigations are required to optimize the angle performance of the gored elbows under different flow conditions and case scenarios.

The 18-degree gored elbow (Design 2) has the highest increase in erosion depth in both cases, suggesting that it is the most vulnerable to the worst-case scenarios. The 22.5-degree gored elbow (Design 3) has the highest decrease in erosion in both cases, indicating that it is the most resistant to the worst-case scenarios. The 30-degree gored elbow (Design 4) has a mixed performance, with an increase in one case and a decrease in another, indicating that is moderately affected by the worst-case conditions. This examination suggests that the angle of the gored elbows plays a significant role in determining the erosion under the worst-case scenarios.

The 22.5-degree gored elbow (Design 3) exhibits the least maximum erosion when compared with all other evaluated cases. This reduced erosion may be attributed to the particles impacting the side wall and the outer curvature of the bend, leading to a distributive collision effect. Specifically, in Design 3, when particles collide with the outer wall, it becomes the primary erosion zone. However, due to the gored section, the particle rebound effect is diminished, resulting in an erosion morphology characterized by less severe erosion on the sidewalls and outer wall.

The shape of the gored elbow, particularly its edges, significantly influences flow patterns and turbulence generations. This aspect is crucial, as regions with reduced turbulence tend to experience increased particle dwell time and subsequent erosion. Design 3, with its distinctive geometry, effectively reduces turbulence in critical zones, potentially through streamlined flow or particle diversion, leading to the notably lower erosion rates observed compared to other designs. Another crucial factor influencing erosion in the gored elbows is the segment angle. The conventional 90-degree elbow experiences concentrated particle impact, leading to significant wear. In contrast, Design 3, features a unique 22.5° angle that deflects particles, promoting sliding and thus minimizing erosion. While Design 2 and Design 4 also provide some deflection and generally less erosion than the standard elbow, their angles may not be as effective as Design 3, potentially resulting in slightly higher erosion rates.

Sand particles travel within an air stream encountering an elbow, they behave like tiny projectiles. Due to their inertia, they tend to continue traveling straight while the airflow curves around the bend. The impacts can be highly erosive, wearing down the material surface over time. The severity of the erosion depends on factors like the velocity of airflow, the size density of the sand particles, and the angle of the elbow. In the context of erosion in elbow pipes, the interaction between sand size, flow rate, and elbow design is critical. As the operating conditions such as velocity and flow rate increase, the kinetic energy of the sand particles also rises, leading to higher erosion rates. The size of the sand particles is a significant factor as large particles tend to have more mass, contributing to greater kinetic energy and thus more severe erosion. However, there is a threshold beyond which the increase in particle size does not extensively affect the erosion rate, as the impact energy becomes less sensitive to changes in particle size.

The impact of flow rate on elbow erosion is also considerable. Higher flow rates result in increased particle kinetic energy, which in turn enhances the erosion rates. This increase in erosion is driven by two main factors related to flow rate. First, higher flow rates elevate the kinetic energy of the particles, making them more erosive. Second, increased flow rate influences the fluid dynamics, and can potentially alter the erosion patterns in elbow geometries.

In the comparative analysis of the elbow designs, the conventional 90-degree elbow (Design 1) is most vulnerable to erosion, largely due to the high velocity impacts it encounters. Conversely, the gored elbow configurations (Designs 2,3 and 4) demonstrate a decline in erosion rates. This improvement is likely a result of their segmented construction, which facilitates a gentler transition of flow. Notably, Design 3, characterized by its 22.5-degree segments, stands out with minimal erosion rates observed. This indicates that such an angle may be more conducive to erosion mitigation. The rationale behind this could be the angle effectiveness in diminishing turbulence and the at which sand particles collide with the elbow interior surfaces, consequently deducing the particles localized velocity and kinetic energy. Thus, the Design 3 configuration appears to be optimal for minimizing erosion within the parameters of this study. Furthermore, gored elbows emerge as a more erosion-resistant design compared to the standard 90-degree elbow,

within an optimal segment angle offering the best protection against erosion.

3.2. Erosion Rate Analysis of Water-Sand Flows.

The results for the water-sand erosion simulation for the four distinct elbow designs, each subjected to various influencing parameters, are represented in Table 7.

Table 7.Maximum erosion rates for different elbow designs and factors in water-sand flow.

Case	Velocity (m/s)	Sand Size (µm)	Flow Rate (Kg/s)	Maximum Erosion Rate Oka (Kg/m2-s)			
				Design 1	Design 2	Design 3	Design 4
1	10	200	0.05	8.273E-06	1.772E-05	1.858E-05	1.634E-05
2	12	225	0.065	1.884E-05	4.926E-05	4.514E-05	4.374E-05
3	15	250	0.08	3.378E-05	9.081E-05	1.181E-04	1.312E-04
4	18	275	0.095	7.069E-05	1.874E-04	2.224E-04	2.494E-04
5	20	300	0.1	8.972E-05	2.125E-04	3.458E-04	3.923E-04

The result shows that in the first case, the conventional 90-degree elbow (Design 1) has the lowest erosion rate, while the 22.5-degree gored elbow (Design 3) has the highest erosion rate. This means that Design 3 is more prone to erosion, while Design 1 is more resistant to erosion effect in the water-sand flows. The table also shows that the 18-degree gored elbow (Design 2) and the 30-degree gored elbow (Design 4) have higher erosion rates than the standard 90-degree elbow. The erosion rates of Design 2 and Design 4 are similar, but Design 2 is slightly higher than Design 4 in terms of erosion susceptibility.

As shown in Table 7, the conventional 90-degree elbow (Design 1) has the lowest erosion rate among all the designs for case 2. In contrast, the 18-degree gored elbow (Design 2) has the highest erosion rate, followed by the 22.5-degree gored elbow (Design 3) and the 30-degree gored elbow (Design 4). These results indicate that the conventional 90-degree elbow is more resistant to erosion than the gored elbows with different angles in the water-sand flows. For cases 3 to 5, all three cases show a similar trend in the erosion rates of different elbow designs. The conventional 90-degree elbow (Design 1) has the lowest erosion rate, while the 30-degree gored elbow (Design 4) has the highest erosion rate. The 18-degree gored elbow (Design 2) and the 22.5-degree gored elbow (Design 3) have intermediate erosion rates, with Design 2 being lower than Design 3. Figure 9 shows the graphical representation of how the erosion rate varies in different designs under different operating conditions.

Figure 9 shows how the erosion rate varies for different elbow designs, in water-sand flows. The conventional 90-degree elbow (Design 1), shown by the blue curve, has the lowest erosion rate in all cases. The other three designs, the 18-degree gored elbow (Design 2) shown by the orange curve, the 22.5-degree gored elbow (Design 3) shown by the black curve, and the 30-degree gored elbow (Design 4), shown by the red curve, have higher erosion rates than the standard 90-degree elbow. The gored elbows have similar erosion rates, with minor fluctuations, in the first two cases. However, from cases 3 to 5, the 30-degree gored elbow (Design 4) has the highest erosion rate, followed by the 22.5-degree gored elbow (Design 3), and the 18-degree gored elbow (Design 2). This indicates that gored elbows are less effective in reducing erosion in water-sand flow. Compared to other designs, the standard 90-degree elbow shows better performance in resisting erosion, even under high-influencing conditions. Hence, the conventional 90-degree elbow is a suitable design for water-sand flows that require high erosion resistance. The average erosion rates for the water sand flow scenario present a clear trend across the designs. Design 1 shows the lowest erosion rate of 4.43E-05 Kg/m²-s, suggesting its resilience in this specific arrangement. In contrast, Design 2, 3 and 4, which contain gored segments, exhibit higher erosion rates. Design 2 average erosion rate is 1.12E-04 Kg/m²-s, while Design 3, despite its lower erosion in air-sand flows, has an increased rate of 1.50E-04, in this context. Design 4 has the highest average rate of 1.67E-04 Kg/m²-s. These results imply that while gored elbow designs may perform better in certain conditions, the standard 90-degree elbow maintains a consistent performance against erosive forces in the water sand environment

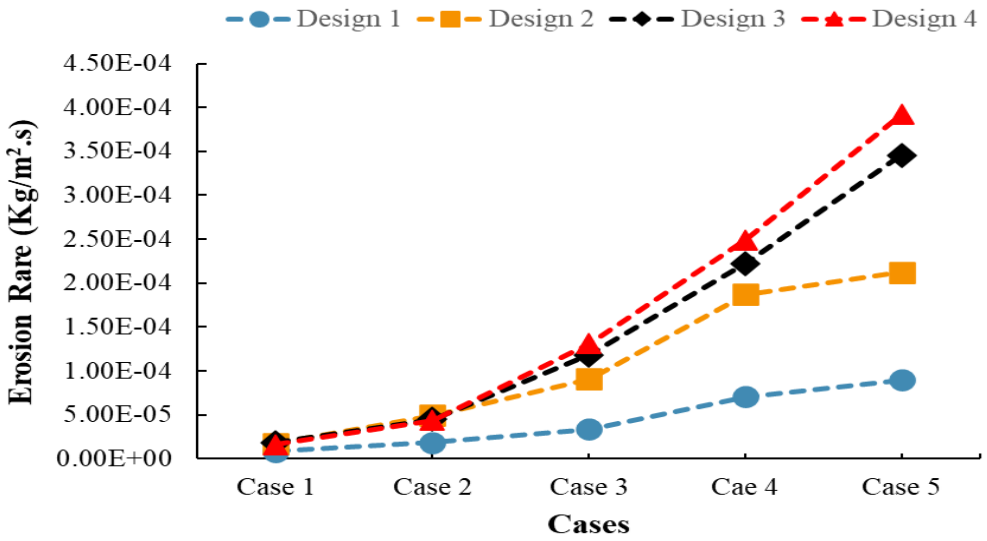

Fig. 9. Erosion rate trends for different elbow designs and water-sand operating conditions.

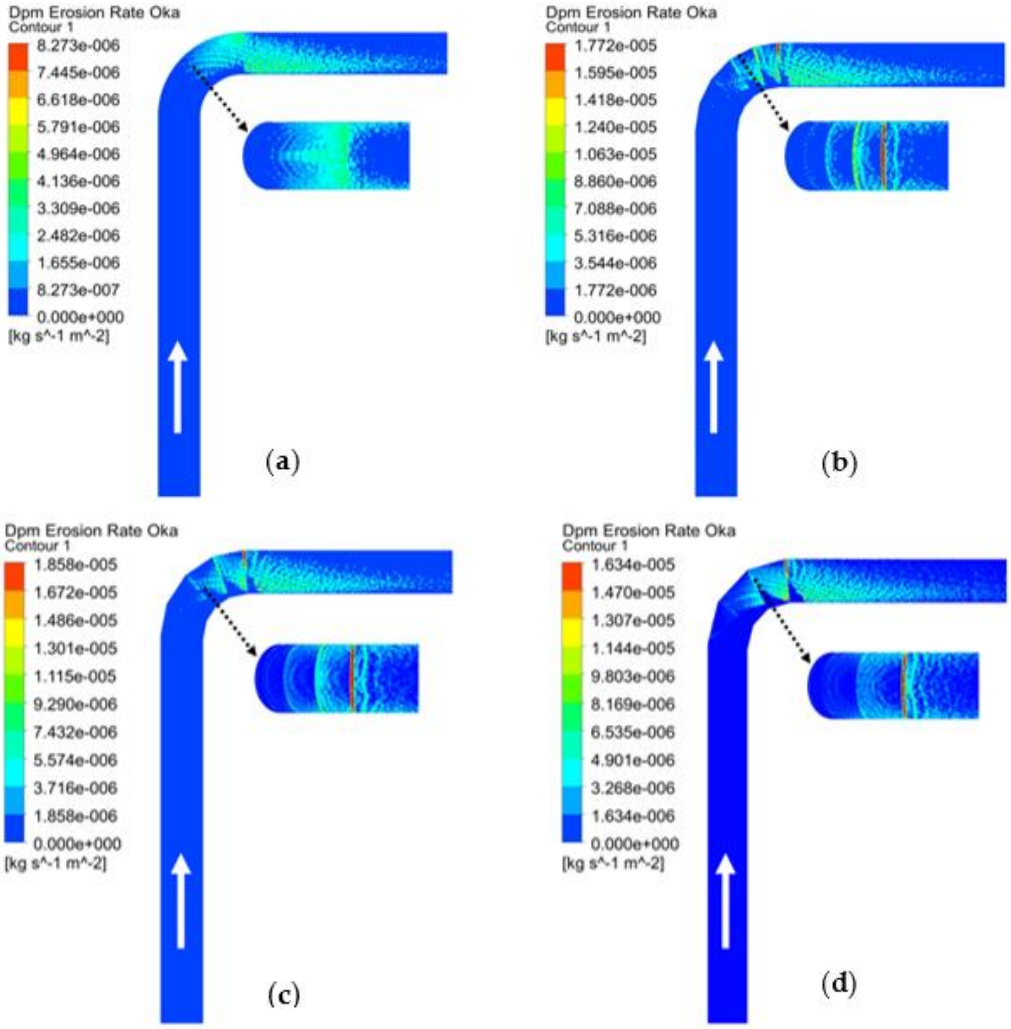

Fig. 10. Erosion rate of the (a) standard 90-degree elbow, (b) 18-degree gored, (c) 22.5-degree gored elbow, (d) 30-degree gored elbow in water-sand flow for the first case (velocity=10 m/s, sand size=200µm, flow rate=0.05 kg/s).

The contour plot in Figure 10 (a) indicates that the erosion rate is highest at the downstream end of the standard 90-degree elbow. The sides of the pipe experience significant erosion, and the elbow experiences the most severe erosion at the point of

flow impact as illustrated by the top view. The erosion pattern in all three gored elbows is identical to the standard 90-degree elbow, however, the gored elbows experience significantly higher erosion at the flow impact. This region is evident in all the gored elbows by the red lines, indicating a severe erosion rate at this point. The edges of the gored elbows, where the segments meet, are the most critical erosion points. In water-sand flow, the sand particles directly impact the edges of the gored elbows, causing significant wear and tear at these locations. The top view of gored elbows as shown in Figure 10 (b), (c), and (d), reveals dispersed erosion points, in contrast to the conventional 90-degree elbow. This difference may be due to the varying impact angles caused by the segments in gored elbows. However, it is clear that gored elbows experience significantly higher erosion rates than the standard 90-degree elbow in water-sand flows. The influencing parameters for the water-sand flow were significantly increased to simulate the worst-case scenario, similar to the air-sand flow. Table 8 shows the maximum erosion rate and the influencing parameters for the two additional cases.

Table 8. Maximum erosion rates in worst-case scenarios for different elbow designs and factors in water-sand flow.

Case	Velocity (m/s)	Sand Size (µm)	Flow Rate (Kg/s)	Maximum Erosion Rate Oka (Kg/s.m2)			
				Design 1	Design 2	Design 3	Design 4
1	30	400	0.2	6.649E-04	1.669E-03	1.903E-03	1.791E-03
2	40	500	0.4	2.584E-03	6.746E-03	8.551E-03	8.932E-03

As shown in Table 8, the standard 90-degree elbow (Design 1) exhibits the best erosion resistance in water-sand flows among all the designs, having minimum erosion in both cases. For the first case, the 22.5-degree gored elbow (Design 3) suffers the most from erosion, followed by the 30-degree gored elbow (Design 4), and the 18-degree gored elbow (Design 2). For the second case, however, the erosion rate is worst for the 30-degree gored elbow (Design 4), followed by the 22.5-degree gored elbow (Design 3), and the 18-degree gored elbow (Design 2). Based on this discussion, it can be concluded that gored elbows are ineffective in reducing the erosion rate in water-sand flows. A graphical representation of the worst-case scenario performance of each design is given in Figure 11.

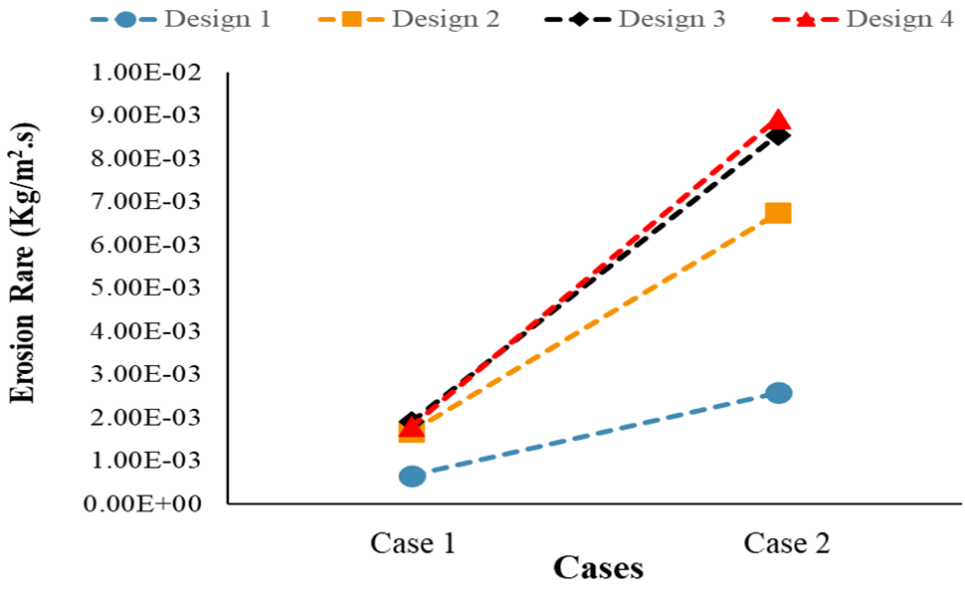

Figure 11. Effect of elbow design on erosion rate in worst-case-scenario water-sand flow.

Figure 11 shows that the 90-degree elbow has significantly lower erosion rates than the gored elbows, even in the worst-case scenario of water-sand flow. This is probably due to its streamlined shape, which reduces the impact of solid particles. In contrast, the edges in the gored elbows make erosion worse, particularly in worst-case scenarios. Therefore, the 90-degree elbow is a better option in water-sand flow applications. The erosion rate of worst-case scenario for case 2 is illustrated in Figure 12.

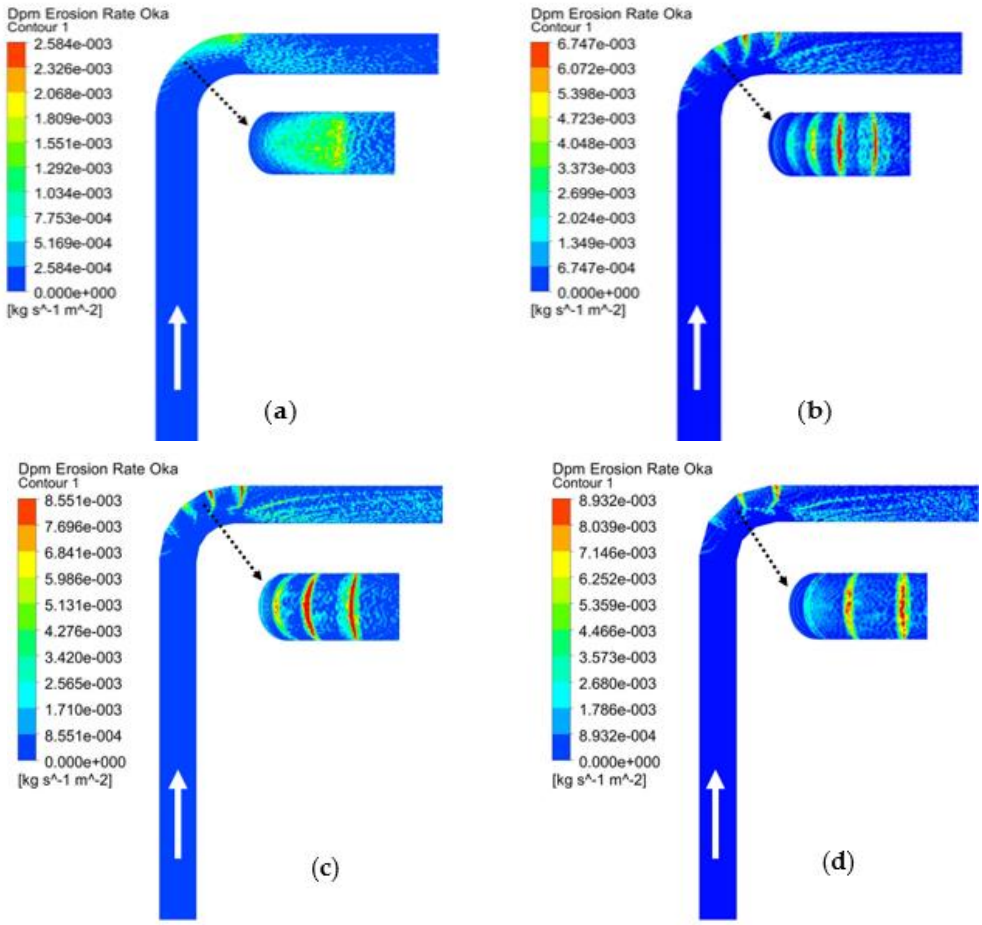

Fig. 12. Erosion rate of the (a) standard 90-degree elbow, (b) 18-degree gored, (c) 22.5-degree gored elbow, (b) 30-degree gored elbow in a worst-case scenario, in water-sand flow (velocity=40 m/s, sand size=500μm, flow rate=0.4 kg/s).

The erosion rate rises sharply as the influencing parameters increase, as Figures 12 demonstrate. This is evident in the erosion spots, especially on the outer surface of the 90-degree elbow and the gored elbow corners are more prone to erosion, as indicated by the red marks. This finding reveals how these components react to different parameters and show the areas where erosion is more intense. Water-sand flows turn gored elbows from erosion protectors to erosion causes. Their curved shapes, which work well in air-sand flows, cause a lot of damage in water-sand flows. The gored elbow shape makes the flow more chaotic, and sand particles spin around and scratch the elbow surface. Vortices and recirculation zones keep these sand particles in place, making some areas more eroded than others.

The gored elbow shape reduces the overall flow rate but increases the flow velocity in some regions. Near the inner wall and the transitions, the flow is constricted, giving more energy to the sand particles. These regions have high erosion rates, where sand particles create deep groves and marks on the elbow surface. At the edges, where the segments are, the flow makes a sharp turn, creating a vortex and a velocity spike. This region also has high erosion rates, where sand particles abrade the elbow surface. Our results show that the 30-degree design, with its large curve, has the highest erosion rate followed by the 22.5-degree and 18-degree designs. The 90-degree elbow, with its simple geometry, has the lowest erosion rate.

The result elucidates the gored elbows have much higher erosion than the standard 90-degree elbow in all cases and that the erosion generally increases with the angle of gored elbows. The data also suggests that the water-sand flows have different effects on erosion depending on each case. All the 18-degree elbow (Design 2), the 22.5-degree gored elbow (Design 3), and the 30-degree gored elbow (Design 4) have the lowest increase in erosion rate in case 1 with 2.14, 2.25, and 1.97 times respectively as the factor of erosion increase. Conversely, the 18-degree gored elbow (Design 2) in case 3 has the highest increase of 2.69 times, while the 22.5-degree gored elbow (Design 3), and the 30-degree gored elbow (Design 4) have an

increase in erosion in case 5 with 3.49 and 4.37 times respectively.

The 30-degree gored elbow (Design 4) has the highest increase in erosion in both cases of the worst-case scenario, implying that it has the most erosion compared to the standard 90-degree elbow (Design 1). The 18-degree gored elbow (Design 2) has the lowest erosion in both cases, indicating the least erosion, while the 30-degree gored elbow (Design 3) has a moderate increase in erosion in both cases, representing a medium erosion increase compared to the standard 90-degree elbow. The increase in erosion demonstrates that the gored elbows are less effective than the standard 90-degree elbow for water-sand flows.

In water-sand flows, higher flow velocities translate to more forceful impacts from sand particles, enhancing the erosion. Similarly, large sand particles carry more kinetic energy, leading to increased wear. Finally, at higher flow rates, more sand particles impact the pipe wall per unit time, intensifying erosion. Essentially, a combination of these parameters determines how quickly the water-sand slurry wears down the pipelines.

Sand particles in water flow have a more complex interaction with the elbow wall. on one hand, water can act as a protective layer. At lower flow rates, the water can moderate the impact of sand particles, reducing their erosive potential. The water essentially absorbs some of the impact energy, lessening the direct blow on the elbow wall. However, water flow can also be a significant contributor to erosion, especially at high velocities. When water carries a high concentration of sand, it transforms into an abrasive slurry. As the fast moving, sand-laden water navigates the elbow, it scours the inner wall. This scouring effect can be particularly damaging, wearing down the material at an accelerated rate. This interaction between water velocity, sand concentration, and elbow design becomes crucial in determining the extent of erosion in this scenario.

Compared to Design 1 (the 90-degree elbow), gored elbows (Designs 2, 3 and 4) experience higher erosion rates in water-sand flows. While Design 1 concentrates the erosive forces on a smaller outer bend area, the gradual turns in gored elbows exposed a large curved section of the wall to the abrasive sand particles. This extended contact with the sand-laden water, even at slightly lower impact forces due to the gentler angle, leads to more erosion in gored designs. Consequently, gored elbows, despite offering some mitigation in air-sand flows compared to the concentrated wear in Design 1, suffer from a higher erosion rate due to the large area exposed to the abrasive flow.

3.3. Particle Track in Air-Sand Flow and Liquid-Sand Flow.

Particle tracking is used in both air-sand and water-sand flows to identify the areas where particle impacts are more or less frequent. Particle tracking also reveals the paths that particles follow after impacting the elbow surface, providing insights into their post-impact trajectories. To comprehensively illustrate the diverse particle paths and behavior within each design, two specific particles were tracked in detail. This in-depth analysis allowed for a subtle understanding of individual particle interactions with the elbow segments. Additionally, the trajectories of a larger number of particles were also tracked to provide a broader perspective on the overall flow patterns and collision frequency within each design.

Figure 13 (a) shows the particle trajectories within the standard 90-degree elbow in air-sand flow. The particle trajectory is shown by two particles that enter the inlet of a 90-degree elbow pipe and follow a straight path until they collide with the elbow wall. The first point of impact for particles 1 and 2 are indicated by a1 and a2, respectively. After the first impact, their paths change and they collide with the elbow wall again at the second points of impact, as shown by b1 and b2, respectively. After impinging on the wall of the 90-degree elbow at a1, Particle 1 undergoes a slight deflection and subsequently strikes the upper wall of the elbow at the second point, b1. It then exits the elbow towards the outlet, following a straight path. Conversely, particle 2, upon impacting the elbow's upper wall at a2, undergoes a rebound at a shallower angle compared to particle 1. This deflection directs it towards the lower side of the pipe where it strikes at point b2. Finally, it exits the pipe through a straight path. Although both particles exhibit high kinetic energy at their initial impact, leading to significant wall abrasion at points a1 and a2, the subsequent collisions, characterized by lower momentum and diverse angles, contribute less to the cumulative erosion rate.

The zoomed-in view of Figure 13 (a) reveals that particle-wall interactions continue beyond the elbow, as evidenced by

the scattered points of impact on the lower pipe wall. The most prominent finding is a significantly higher concentration of particles impacting the extrados, causing the most severe wear and tear. Conversely, the intrados experiences minimal impact, forming a region with markedly lower erosion. This is further visualized by the side view of the elbow pipe where the dotted box highlights the area receiving the majority of particle strikes. These diverse impact points directly manifest as distinct erosion patterns. Some particles in the elbow strike the extrados, rebound, and hit the lower wall, while the intrados remains largely untouched, highlighting a vast area with no particle impact.

Figure 13 (b) illustrates the distinct particle trajectories within the 18-degree gored elbow. The particle trajectories in the 18-degree gored elbow are initially similar to those in the standard 90-degree elbow, but the impact points and post-impact regions differ significantly. Particle 1 strikes the second segment of the 18-degree gored elbow at point a1, and due to the inclination of the segment, the particle experiences a deflection and hits the upper wall at point b1 at a slightly longer distance than in the 90-degree elbow. At point b1 the particle is again deflected from the last segment of the elbow and collides with the lower wall of the pipe at point c1 at a longer distance, and then moves to the outlet of the elbow without further encounter with the wall. The path of particle 2 after the first collision with the wall at point a2 slightly bends in the upward direction where it hits the side of the pipe at point b2. The rebound of particle 2 directs it to the lower wall at c2, similar to particle 1 before exiting.

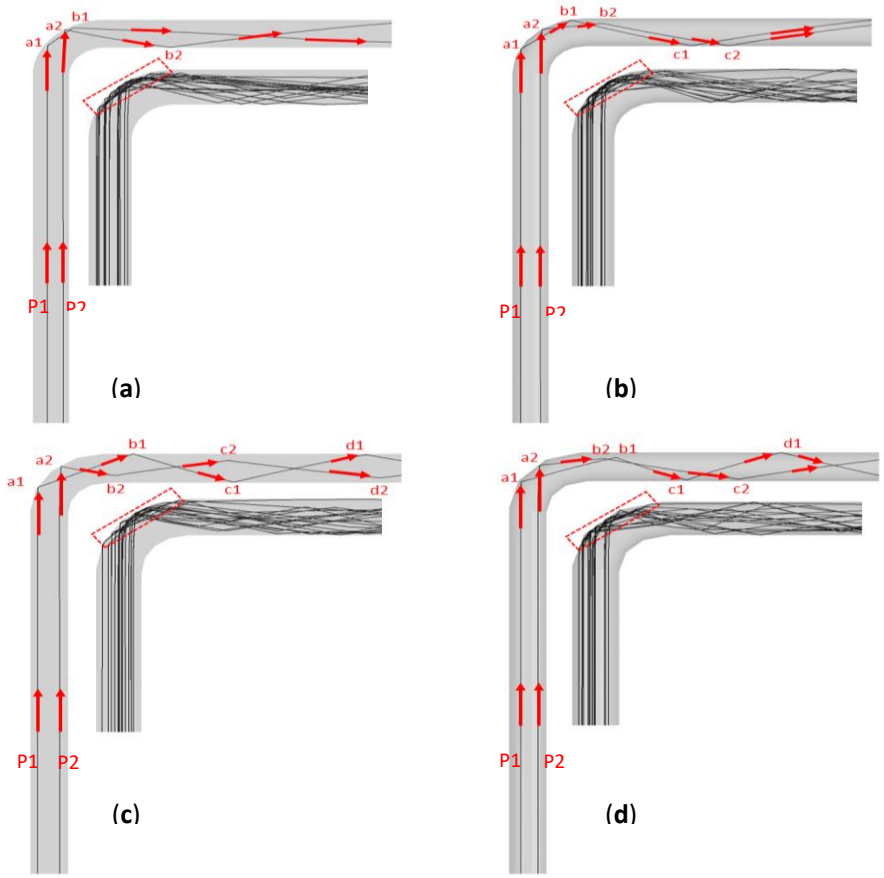

Fig. 13. Particle track for air-sand flow in (a) standard 90-degree elbow, (b) 18-degree gored elbow, (c) 22.5-degree gored elbow, (d) 30-degree gored elbow.

The zoomed-in view reveals that the extrados experiences extreme particle impacts, contributing to higher erosion, while the intrados remain intact. The segment inclination significantly affects the paths of the particles, causing them to hit the lower wall at different locations as shown in Figure 13 (b). Compared to the standard 90-degree elbow, the 18-degree gored elbow experiences a higher number of particles colliding with the lower wall. Additionally, the segments in the 18-degree gored elbow distribute particle impacts instead of concentrating them in specific locations. This distribution also reduces the erosion

rate and directs some particles toward the upper wall, receiving a portion of the particle impact.

Figure 13 (c) and (d) illustrate the contrasting particle trajectories within the 22.5-degree and 30-degree gored elbows. In the 22.5-degree case (Figure 13 (c)), particle paths become significantly more erratic after the initial collision. Particle 1, highlighted in Figure 13 (c), initially follows a straight path before hitting the lower part of the second segment of the elbow at point a1. It then deflects off the elbow surface, striking the upper wall at b1. Particle 1 then rebounds from this point, hitting the lower wall at c1. Another rebound guides it back to the upper wall, where it strikes at d1 before exiting the outlet.

Particle 2 (Figure 13(c)), takes a different path compared to particle 1. It initially strikes the third segment of the 22.5-degree gored elbow at a2. This segment angle guides particle 2 towards the lower portion of the pipe, causing it to collide with the wall at b2. It then rebounds from this point and strikes the pipe again at two distinct locations, c2 and d2. Both follow a zigzag pattern, colliding with the outlet pipe wall at multiple locations, unlike the 90-degree case where impacts are concentrated. This helps to reduce the erosion rate considerably in the 22.5-degree gored elbow due to the segment position in this design.

The 22.5-degree gored elbow causes particles to rebound from the extrados and hit the adjacent part of the lower wall of the elbow pipe. This behavior is primarily due to the orientation of the third segment within the gored elbow design. Observing the side view (Figure 13(c)), it is evident that many particles also impact the upper wall of the pipe. This can be attributed to the deflection of particles caused by the first and second segments. Overall, the 22.5-degree gored elbow's third segment orientation significantly alters the particle trajectories compared to the standard 90-degree elbow. This results in a more dispersed distribution of impacts on both the upper and lower walls of the pipe, potentially contributing to reduced erosion in specific areas.

The 30-degree gored elbow exhibits a broadly similar impact pattern as the 22.5-degree gored elbow with subtle deviations after the first encounter. Particles 1 and 2 initially impact at point a1 and a2 (Figure 13 (d), as with the 22.5-degree case. However, their rebounds differ slightly. In the 30-degree case, particle 1 exhibits a near identical rebound angle to the 22.5-degree case, striking the upper surface at b1. Particle 2, however, diverges significantly. Its rebound angle differs, propelling it towards the upper wall for impact at b2, unlike the lower wall impact seen in the 22.5-degree case. Following this, the trajectories diverge further. Particle 1 deflects again and hits the lower wall at c1 before striking the upper wall at d1. In contrast, particle 2 hits the lower wall at c2 but exits the pipe without further interactions. This highlights the dynamic interplay between segment angles and particle paths within the 30-degree gored elbow. Figure 13 (d) reveals dispersed particle impacts on the outlet pipe in the 30-degree elbow. This, driven by the gored elbow segment angle, spreads particle impact, potentially reducing concentrated wear compared to a standard 90-degree elbow. It is worth noting that factors beyond the elbow geometry, such as fluid properties, mass flow rate, and velocity, also influence the impact points and intensity. These aspects contribute to shaping the overall erosion patterns and particle transport within the fluid.

As Figure 14 shows, water properties have a significant influence on the trajectories of water-sand flows.

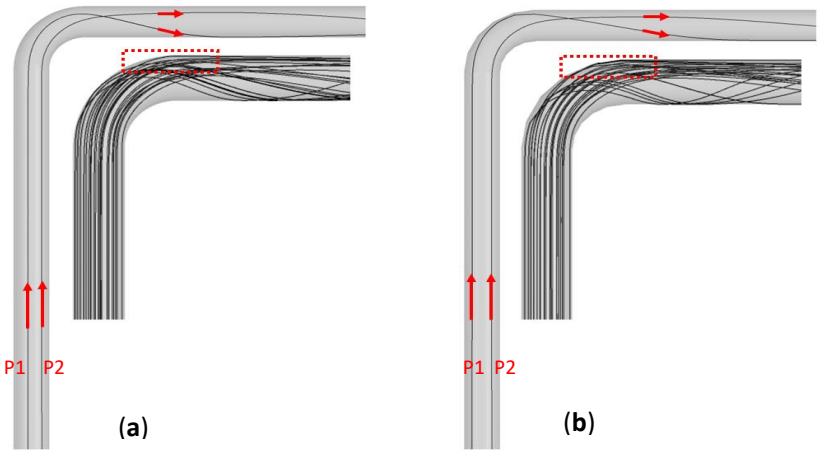

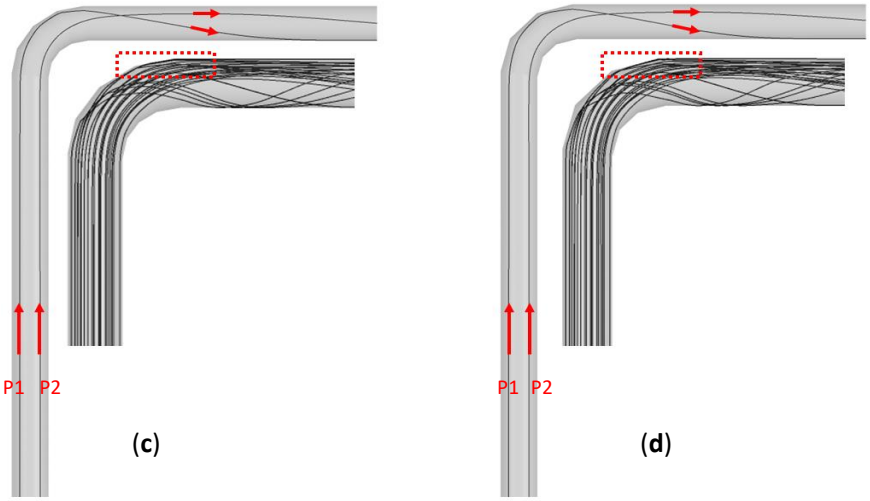

Fig. 14. Particle track for water-sand flow in (a) standard 90-degree elbow, (b) 18-degree gored elbow, (c) 22.5-degree gored elbow, (d) 30-degree gored elbow.

When two particles enter a standard 90-degree elbow, they initially follow straight paths until they reach the bend as Figure 14 (a) illustrates. At this point, their trajectories change. Particle 1 curves sharply, and impacts the lower wall at some distance from the elbow before exiting directly. Particle 2, on the other hand, follows a gentler curve towards the upper wall, crossing the path of particle 1. Particle 1 keeps its slight curvature and exits without further collision. Figure 14 (a) also shows the trajectories of a large number of particles in the standard 90-degree elbow. The outer surface near the end of the elbow which is highlighted by a dotted box, has the highest erosion rate in the water-sand flow. Some particles rebound from this surface and hit the lower wall of the pipe, while other particles move straighter and exit the pipe. Some particles curve towards the sides of the pipe and collide with the wall, resulting in erosion. The particle trajectories in the 18-degree gored elbow are illustrated in Figure 14 (b). The trajectories of the two particles resemble those in the standard 90-degree elbow, but particle 1 is closer to the bend in the 18-degree gored elbow. More particles hit the segment edges, causing severe erosion. Some particles rebound from the edges and hit the lower pipe wall at different positions. The segments in the 18-degree gored elbow disturb the particle paths, which deviate from those in the 90-degree elbow. The 22.5-degree and 30-degree gored elbows have similar particle trajectories as the 18-degree ones, with more impacts on the segment edges as shown in Figures 14 (c) and (d). Particles also collide with various positions along the pipe sides, with a relatively small number following a straight path to the outlet. The water properties affect the particles' paths to vary from those in air flow.

Figure 14 demonstrates a significant reduction in particle collisions in water-sand flows as opposed to those in air-sand flows shown in Figure 13. Nevertheless, elements such as the behavior of the fluid and the characteristics of the particles also play an essential role in the observed erosion rate differences.

Air-sand flows are marked by a higher frequency of particle collisions, which significantly contribute to erosion. However, the lower density of air relative to water results in decreased particle impact velocities. This leads to weaker collision forces against the pipe wall, resulting in less wear per collision compared to denser fluid flows like water-sand, even when the particle mass is consistent. On the other hand, water-sand flows may have fewer collisions, but the impacts could be more forceful due to the greater density of water. Moreover, the viscous nature of water may cause particles to linger and drag along the pipe surface, resulting in more significant erosive damage than in air-sand flows, despite a reduced number of particles. To understand the erosion rate discrepancies between water-sand and air-sand flows, a thorough analysis is essential. It should evaluate the collision frequency and the distinct particle-fluid interactions, alongside the pipe design and material properties.

4. Conclusions

This study aimed to investigate the erosion caused by multiphase air-sand and water-sand flows in various elbow

designs, and to identify the optimal design and operating conditions to mitigate erosion. The designs include a standard 90-degree elbow, 18-degree gored elbow, 22.5-degree gored elbow, and 30-degree gored elbow. The performance of all the designs was investigated under a range of operating conditions, including fluid velocities, sand sizes, and sand flow rates. The erosion phenomenon and its influencing factors were investigated by CFD simulations for different elbow geometries. The fluid velocity varied from 10 to 40 m/s, the particle size varied from 200 to 500 μm, and the sand flow rate varied from 0.05 to 0.4 kg/s, to identify the optimal elbow design and mitigate erosion. The main findings of this study are presented in detail in the following sections.

1. The results show that the gored elbows outperformed the standard 90-degree elbow in reducing erosion, with the 22.5-degree gored elbow showing the most consistent decrease of up to 32%. While the 18-degree and the 30-degree gored elbows exhibit erosion reduction, their performance was less consistent, with an 18-degree design showing an erosion increase of up to 1.32 times and the 30-degree configuration showing an increase of up to 1.06 times the baseline respectively. Overall, the study suggests that gored elbows particularly the 22.5-degree design, offer a promising approach for reducing erosion in air sand flows.
2. The gored elbow designs display different erosion scars, compared to the 90-degree elbow, which has an elliptical and V-shaped erosion scar, influenced by the impact points and concentrations of sand particles. The 18-degree gored elbow has a curved rectangular scar with scattered points at the sides and upper portion of the elbow, the 22.5-degree gored elbow has a cylindrical scar similar to a semicircular closed arch, and the 30-degree gored elbow has a trapezium-shaped scar and dispersed erosion points at the sides and upper part of the elbow.
3. The gored elbows, regardless of angle, were ineffective in mitigating erosion in water-sand flows. All gored elbow designs (18-degree, 22.5-degree, and 30-degree) exhibited significantly higher erosion rates than the standard 90-degree elbow under all water-sand flow conditions. Furthermore, the erosion rate generally increased with the angle of the gored elbow, with a 30-degree gored elbow experiencing the most severe erosion in most cases. These findings suggest that alternative strategies may be necessary for erosion control in water-sand flows.
4. The particle trajectories and impact points in air-sand flows vary across different elbow geometries. Gored elbows, unlike standard 90-degree design, induce diverse particle impacts due to segmented arrangements. The segment angles in gored elbows substantially influence impact distribution and erosion locations. This is achieved through higher collision rates and segment-driven trajectory variations.

This study suggests erosion mitigation on pipelines by using the gored elbow over the standard 90-degree elbows in gas-solid flow conditions. It is recommended to conduct experimental investigations on the gored elbows and analyze the erosion rate and locations of high impact points. This would verify the numerical models and examine the geometrical effects on the erosion of gored elbows. Spherical particles were assumed in the numerical investigations, but sand particles have a variety of sizes and irregular shapes in reality. Therefore, both experimental and numerical investigations on the performance of different elbow designs using realistic sand particles are recommended.

Acknowledgments

The authors would like to acknowledge the Researchers Supporting Project number (RSPD2024R597), King Saud University, Riyadh, Saudi Arabia.

References

1. Beyralvand D, Banazadeh F, Moghaddas R. Numerical investigation of novel geometric solutions for erosion problem of standard elbows in gas-solid flow using CFD-DEM. Results in Engineering. 2023;17:101014. https://doi.org/10.1016/j.rineng.2023.101014
2. Huang J, Wen J, Li H, Xia Y, Tan S, Xiao H, Duan W, Hu J. Particle erosion in 90-Degree elbow pipe of pneumatic conveying System: Simulation and validation. Computers and Electronics in Agriculture. 2024;216:108534. https://doi.org/10.1016/j.compag.2023.108534

3. Li Z, Wei X, Yi Z, Ma Z, Yu Y, Wang W. Numerical analysis of gas-liquid-solid erosion characteristics of the oil and gas multiphase pump. Engineering Failure Analysis. 2024;157:107889. https://doi.org/10.1016/j.engfailanal.2023.107889
4. Lin N, Arabnejad H, Shirazi SA, McLaury BS, Lan H. Experimental study of particle size, shape and particle flow rate on Erosion of stainless steel. Powder Technology. 2018;336:70-9. https://doi.org/10.1016/j.powtec.2018.05.039
5. Li A, Wang Z, Zhu L, Wang Z, Shi J, Yang W. Design optimization of guide vane for mitigating elbow erosion using computational fluid dynamics and response surface methodology. Particuology. 2022;63:83-94. https://doi.org/10.1016/j.partic.2021.02.006
6. Liu Xq, Liu F, Ji H, Li N, Wang C, Lin G. Particle erosion transient process visualization and influencing factors of the hydraulic servo spool valve orifice. Flow Measurement and Instrumentation. 2023;89:102273. https://doi.org/10.1016/j.flowmeasinst.2022.102273
7. Yao L, Liu Y, Xiao Z, Feng Z. Investigation on tee junction erosion caused by sand-carrying fracturing fluid. Tribology International. 2023;179:108157. https://doi.org/10.1016/j.triboint.2022.108157
8. Basyouny A. Experimental validation of numerical two-phase flow in a horizontal separator. Results in Engineering. 2022;15:100476. https://doi.org/10.1016/j.rineng.2022.100476
9. Zhao X, Cao X, Zhang J, Cao H, Xie Z, Xiong N. Numerical investigation and dimensionless erosion laws of solid particle erosion in plugged tees. Powder Technology. 2022;402:117342. https://doi.org/10.1016/j.powtec.2022.117342
10. Mazumder QH. S-bend erosion in particulated multiphase flow with air and sand. The Journal of Computational Multiphase Flows. 2016;8(3):157-66. https://doi.org/10.1177/1757482X16668363
11. Khan R, Mourad AHI, Seikh AH, Petru J, H.Ya H. Erosion impact on mild steel elbow pipeline for different orientations under liquid-gas-sand annular flow. Engineering Failure Analysis. 2023;153:107565. https://doi.org/10.1016/j.engfailanal.2023.107565
12. Khan R, H. Ya H, Pao W, Majid MAA, Ahmed T, Ahmad A, Alam MA, Azeem M, Iftikhar H. Effect of Sand Fines Concentration on the Erosion-Corrosion Mechanism of Carbon Steel 90° Elbow Pipe in Slug Flow. Materials. 2020;13(20):4601. https://doi.org/10.3390/ma13204601
13. Solnordal CB, Wong CY, Boulanger J. An experimental and numerical analysis of erosion caused by sand pneumatically conveyed through a standard pipe elbow. Wear. 2015;336-337:43-57. https://doi.org/10.1016/j.wear.2015.04.017
14. Mazumder QH, Shirazi SA, McLaury BS, Shadley JR, Rybicki EF. Development and validation of a mechanistic model to predict solid particle erosion in multiphase flow. Wear. 2005;259(1):203-7. https://doi.org/10.1016/j.wear.2005.02.109
15. Kesana NR, Grubb SA, McLaury BS, Shirazi SA. Ultrasonic Measurement of Multiphase Flow Erosion Patterns in a Standard Elbow. Journal of Energy Resources Technology. 2013;135(3). https://doi.org/10.1115/1.4023331
16. Abduljabbar A, Mohyaldinn ME, Younis O, Alghurabi A, Alakbari FS. Erosion of sand screens by solid particles: a review of experimental investigations. Journal of Petroleum Exploration and Production Technology. 2022;12(8):2329-45. https://doi.org/10.1007/s13202-022-01467-4
17. Parsi M, Najmi K, Najafifard F, Hassani S, McLaury BS, Shirazi SA. A comprehensive review of solid particle erosion modeling for oil and gas wells and pipelines applications. Journal of Natural Gas Science and Engineering. 2014;21:850-73. https://doi.org/10.1016/j.jngse.2014.10.001
18. Peng W, Ma L, Wang P, Cao X, Xu K, Miao Y. Experimental and CFD investigation of flow behavior and sand erosion pattern in a horizontal pipe bend under annular flow. Particuology. 2023;75:11-25. https://doi.org/10.1016/j.partic.2022.06.003
19. Xiao F, Luo M, Huang F, Zhou M, An J, Kuang S, Yu A. CFD–DEM investigation of gas-solid flow and wall erosion of vortex elbows conveying coarse particles. Powder Technology. 2023:118524. https://doi.org/10.1016/j.powtec.2023.118524
20. Liu J, BaKeDaShi W, Li Z, Xu Y, Ji W, Zhang C, Cui G, Zhang R. Effect of flow velocity on erosion–corrosion of 90-degree horizontal elbow. Wear. 2017;376-377:516-25. https://doi.org/10.1016/j.wear.2016.11.015
21. Duarte CAR, de Souza FJ, dos Santos VF. Mitigating elbow erosion with a vortex chamber. Powder Technology. 2016;288:6-25. https://doi.org/10.1016/j.powtec.2015.10.032
22. Zhu H, Li S. Numerical analysis of mitigating elbow erosion with a rib. Powder Technology. 2018;330:445-60. https://doi.org/10.1016/j.powtec.2018.02.046
23. Zhou H, Zhang Y, Bai Y, Zhao H, Lei Y, Zhu K, Ding X. Study on reducing elbow erosion with swirling flow. Colloids and Surfaces A: Physicochemical and Engineering Aspects. 2021;630:127537. https://doi.org/10.1016/j.colsurfa.2021.127537

24. Duarte CAR, de Souza FJ, Venturi DN, Sommerfeld M. A numerical assessment of two geometries for reducing elbow erosion. Particuology. 2020;49:117-33. https://doi.org/10.1016/j.partic.2019.01.004
25. Duarte CAR, de Souza FJ. Innovative pipe wall design to mitigate elbow erosion: A CFD analysis. Wear. 2017;380-381:176-90. https://doi.org/10.1016/j.wear.2017.03.015
26. Vieira RE, Mansouri A, McLaury BS, Shirazi SA. Experimental and computational study of erosion in elbows due to sand particles in air flow. Powder Technology. 2016;288:339-53. https://doi.org/10.1016/j.powtec.2015.11.028
27. Oka YI, Okamura K, Yoshida T. Practical estimation of erosion damage caused by solid particle impact: Part 1: Effects of impact parameters on a predictive equation. Wear. 2005;259(1):95-101. https://doi.org/10.1016/j.wear.2005.01.039